AIAA 2002-4875

Simulation and Flight Control of an Aeroelastic Fixed Wing Micro Aerial Vehicle

Martin R. Waszak and John B. Davidson
NASA Langley Research Center
Hampton, VA 23681-2199

Peter G. Ifju
University of Florida
Gainesville, Florida 32611-6250

AIAA Atmospheric Flight Mechanics Conference
5–8 August 2002
Monterey, CA

SIMULATION AND FLIGHT CONTROL OF AN AEROELASTIC FIXED WING MICRO AERIAL VEHICLE

Martin R. Waszak* and John B. Davidson†
NASA Langley Research Center, Hampton, Virginia
Peter G. Ifju‡
University of Florida, Gainesville, Florida

Abstract

Micro aerial vehicles have been the subject of continued interest and development over the last several years. The majority of current vehicle concepts rely on rigid fixed wings or rotors. An alternate design based on an aeroelastic membrane wing has also been developed that exhibits desired characteristics in flight test demonstrations, competition, and in prior aerodynamics studies. This paper presents a simulation model and an assessment of flight control characteristics of the vehicle. Linear state space models of the vehicle associated with typical trimmed level flight conditions and which are suitable for control system design are presented as well. The simulation is used as the basis for the design of a measurement based nonlinear dynamic inversion control system and outer loop guidance system. The vehicle/controller system is the subject of ongoing investigations of autonomous and collaborative control schemes. The results indicate that the design represents a good basis for further development of the micro aerial vehicle for autonomous and collaborative controls research.

Introduction

Micro aerial vehicles, or "MAVs", are typically designated as a class of aircraft with a maximum dimension of 6 inches that are capable of operating at speeds of 25 mph or less.[1] Developments in miniaturized digital electronics, communications, and computer technologies and strong support by DARPA have moved the prospect of very small autonomous flight vehicles from the realm of science fiction to science fact. The goal is for these vehicles to provide inexpensive and expendable platforms for surveillance and data collection in situations where larger vehicles are not practical. For example, they can be used for battlefield surveillance or mapping the extent of chemical/radiation spills or viral outbreaks. Other applications include use in search and rescue operations, traffic/news coverage, and crop or wildlife monitoring. Many potential uses would require cooperative and collaborative control capabilities so that large numbers of MAVs could be used to cover a large operational area. In these types of applications MAVs could be coordinated from a central base station or used in collaborative swarms to collect and transmit data.

The research and development required for developing MAVs and related systems is technically challenging and requires a number of technological advances that may benefit a broad range of aerospace applications. The development of a vehicle could also foster development of component technologies and help to support an emerging growth market for micro aerial vehicles.

An aeroelastic fixed wing micro aerial vehicle concept has been developed by a team at the University of Florida with a goal to design a vehicle that could win the ISSMO (International Society of Structural and Multidisciplinary Optimization) Micro Aerial Vehicle Competition; a goal that has been accomplished each of the last four years.[2,3]

The vehicle exploits an innovative aeroelastic wing with the ability to adapt to atmospheric disturbances

---

* Senior Research Engineer, Dynamics and Control Branch. Senior Member AIAA.
† Senior Research Engineer, Dynamics and Control Branch. Senior Member AIAA.
‡ Associate Professor, Department of Aerospace, Mechanics, and Engineering Sciences.

Figure 1 – photograph of Univ. of Florida MAV.

and provide smoother flight thereby providing a better surveillance platform and making the vehicle easier to fly. This is accomplished via a passive adaptive washout mechanism.

The adaptive washout technique has been taken from sailing vessels which use sail twist to greatly extends the wind range of the sail and produce more constant thrust (lift) in gusty wind conditions. Adaptive washout is produced in the MAV by deformation of the membrane wing in response to changes in speed and vehicle attitude. The result produces changes in wing camber and angle of attack along the span. The effect is to reduce the sensitivity of the vehicle to disturbances.

NASA is collaborating with the University of Florida to develop an understanding of the underlying physical phenomena associated with the vehicle concept with a goal of enhancing the vehicle design and developing a capability for investigating autonomous and collaborative control technologies.

Reference 4 documents the results of a wind tunnel test in which aerodynamic data was collected to provide a database to support the development of a dynamic simulation of the University of Florida MAV (UFMAV) concept. In that paper the flexible membrane wing was shown to significantly increase the stall angle of the vehicle without sacrificing L/D ratio. The vehicle was also determined to be statically stable in all axes.

This paper describes the development of a dynamic simulation and flight control assessment based on the aerodynamic data described in reference 4. A control/guidance system design is also presented. The inner loop controller design uses measurement-based nonlinear dynamic inversion. The structure of the guidance system allows the vehicle to be integrated into an existing multiple vehicle collaborative control scheme.[5]

Table 1 – UFMAV geometric and mass properties.

Empty Weight	0.12 lbs
Wing Area	19.8 in^2
Span	6 in
Mean Chord	3.3 in
Moments of Inertia:	
Ixx	0.086 $lb\text{-}in^2$
Iyy	0.23 $lb\text{-}in^2$
Izz	0.21 $lb\text{-}in^2$
Ixz	0.037 $lb\text{-}in^2$

Vehicle Description

The University of Florida MAV (UFMAV) incorporates a high mounted flexible membrane wing and low mounted cruciform tail attached to a tapered fuselage with rectangular cross section (see figure 1). The fuselage is a truss-like design constructed of a carbon fiber/epoxy material covered with a thin transparent monofilm membrane. A more detailed description of the vehicle and its construction can be found in reference 3. Table 1 summarizes the pertinent geometric and mass properties of the vehicle.

A unique aspect of the vehicle is its flexible membrane wing. The cambered wing structure is constructed of unidirectional carbon fiber prepreg laminate forming a leading edge spar and chordwise ribs or battens. A membrane material is bonded to the spar and batten. The wing membrane material is a 4 mil thick flexible latex membrane.

The maximum dimension (including length and wing span) of the vehicle is six inches. The wing area is approximately 19.8 square inches. The root chord is 4.25 inches and the mean chord is 3.3 inches. The camber of the unloaded wing is approximately 6.5 percent of the root chord with the maximum camber occurring at approximately 30 percent chord and is uniform across the span. The wing is mounted at an incidence of approximately nine degrees with wing incidence defined as the angle between the root chord line and the longitudinal axis of the fuselage.

Control is accomplished using two independently controlled elevons that are actuated symmetrically and antisymmetrically using small rotary servos. A small gas engine normally provides propulsion with a three inch diameter propeller with a pitch of 1.25. However, an electric motor was used during wind tunnel tests to more accurately control propeller rpm and is used in the simulation model as well.

Simulation Model

The simulation model is based on the aircraft equations of motion presented in Reference 6. The equations of motion were coded using Matlab/Simulink.[7] The structure of the simulation is depicted in Figure 2. The simulation is structured using subsystems representing actuator dynamics, equations of motion (EOMs), and sensor dynamics. A more detailed block diagram appears in the Appendix.

The actuators subsystem currently consists of first order actuator transfer functions and limiters that bound the permissible range of symmetric δ_{sym} and antisymmetric δ_{asy} control surface deflections (±25 degrees and ±20 degrees, respectively) and commanded motor voltage (0 – 20 volts). The sensor subsystem currently contains no dynamics but will permit sensor models to be added at a later time.

The equations of motion include the longitudinal and lateral-directions equations of motion, models for thrust and aerodynamic forces and moments, and a standard atmosphere model (see Figure 3 and the Appendix). Each of the major components of the EOMs subsystem will be described subsequently.

Equations of Motion

The equations of motion are implemented in two major subsystems representing the vehicle dynamics in the longitudinal and lateral-directional axes. There is coupling between these two subsystems due to inertial and gravitational coupling. There are also several quantities that are used to determine the aerodynamic forces and moments (e.g., body rates, angle of attack, sideslip angle, speed). These quantities are fed back to the aero model as necessary.

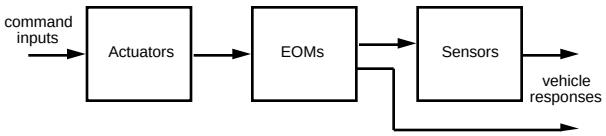

Figure 2 – UFMAV simulation structure.

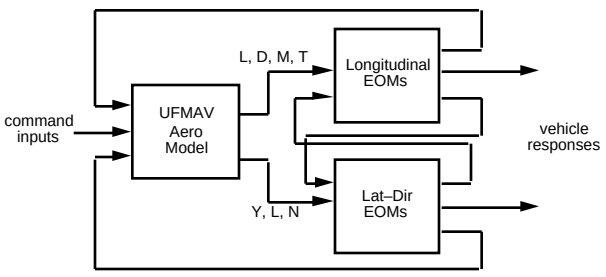

Figure 3 – EOMs subsystem structure.

The longitudinal and lateral-directional subsystems consist of additional subsystems that systematically build up the equations of motion as derived in reference 6. The equations represent the six degree-of-freedom motion of a rigid aircraft relative to a flat, non-rotating earth. The atmosphere is represented using the 1976 Standard Atmosphere model. [6]

UFMAV Aero Model

The aerodynamic model was obtained primarily from wind tunnel data collected in the NASA Langley Basic Aerodynamics Research Tunnel (BART).[4] Linear regression analysis was used to generate functions that approximate the dependence of the forces and moments on angle of attack, sideslip angle, and propeller rpm. The functions are in the form of Taylor series.

The regression analysis was performed using wind tunnel data that consists of the aerodynamic force and moment coefficients at various combinations of angle of attack, sideslip angle, control surface deflection, dynamic pressure, and motor rpm. The range of variation for these parameters correspond to the region over which the aerodynamics are linear.[4] The main implication of this simplification is that the angle of attack is limited to values below 20 degrees and sideslip to values between –5 and 5 degrees. Cross terms between angle of attack, control deflection, and motor rpm are used to account for the dependence on propeller slipstream effects and the effect angle of attack has on control effectiveness. The values of the coefficients are shown in the tables in the Appendix.

Note that there are three sets of coefficients for lift, drag, and pitching moment. Each set corresponds to a different dynamic pressure. The differences are attributable to Reynolds number effects. Interpolation is used in the simulation to determine the coefficient values at any given dynamic pressure between 1.0 and 2.0 psf. Lack of sufficient lateral-direction force and moment data and higher levels of uncertainty for these quantities made it impossible to isolate Reynolds number effects for side force, rolling and yawing moment coefficients. As a result, the values for the lateral-directional coefficients represent an average over dynamic pressure.

Additional terms were added to the Taylor series in an ad hoc manner to account for dependence on angular rates (i.e., dynamic derivatives). Terms associated with the angle of attack and pitch rates were added for lift ($C_{L_q}, C_{L_{\dot{\alpha}}}$) and pitching moment ($C_{M_q}, C_{M_{\dot{\alpha}}}$). Terms associated with roll and yaw rates were added for the side force (C_{Y_p}, C_{Y_r}), rolling moment (C_{l_p}, C_{l_r}) and yawing moment (C_{n_p}, C_{n_r}). The

coefficients for most of these terms were computed using PMARC. [8] Two exceptions were the dynamic derivatives associated with rate of change of angle of attack ($C_{L_{\dot{\alpha}}}, C_{M_{\dot{\alpha}}}$) which were chosen based on "typical" values published in reference 9, page 19. The values for all the dynamic derivatives are shown in the tables in the Appendix.

The expression for total lift force coefficient is shown in equation (1) as an example of the Taylor series expansion.

$$C_L = \left(C_{L_0} + C_{L_T} T\right) + \left(C_{L_\alpha} + C_{L_{\alpha T}} T\right)\alpha + \left(C_{L_{\delta_{sym}}} + C_{L_{\delta_{symT}}} T\right)\delta_{sym} + C_{L_q}\left(\frac{c}{2V}\right)q + C_{L_{\dot{\alpha}}}\left(\frac{c}{2V}\right)\dot{\alpha} \quad (1)$$

The thrust dependent cross terms $C_{L_{(\cdot)T}}$ account for the fact that the effects of thrust are coupled with angle of attack and control surface deflection through prop stream effects. The expressions for drag, side force, and pitching, rolling, and yawing moments are similar in structure but differ in the particular coefficients associated with coupling.

UFMAV Propulsion Model

The propulsion model was obtained from wind tunnel data collected during the BART test.[4] Motor thrust was approximated by subtracting the prop-off axial force from the prop-on axial force. Regression analysis was used to generate generalized Taylor series functions that approximate the dependence of motor thrust on angle of attack, dynamic pressure, and voltage commands. The propulsion model consists of two parts: a motor model that characterizes the relationship between motor voltage command and propeller rpm, and a thrust model that characterizes the relationship between propeller rpm and thrust coefficient. This implementation separates the effect of propeller loading on motor rpm from the thrust produced at a given rpm.

The regression analysis was performed in an ad hoc manner to identify a combination of parameters that provide a reasonable approximation to experimental data. The function approximating the relationship between motor voltage and motor rpm is

$$KRPM = C_{M_0} + C_{M_{\bar{q}}}\bar{q} + C_{M_\alpha}\alpha + C_{M_{\alpha^2}}\alpha^2 + C_{M_{v_{motor}}} v_{motor} + C_{M_{v^2_{motor}}} v^2_{motor} \quad (2)$$

where *KRPM* represents rpm/1000. Note that the behavior is essentially quadratic in motor voltage (v_{motor}) with a variable offset which is determined by propeller loading effects expressed through a dynamic pressure ($\bar{q}$) dependent term and the angle of attack dependent terms.

The function relating thrust to motor rpm is

$$C_T = \left(C_{T_1} + C_{T_2} KPRM\right)\left(\frac{KRPM}{\bar{q}}\right)^2 \quad (3)$$

where C_T is the thrust coefficient. No attempt was made to explain the structure of this equation on a physical basis. Tables of the propulsion model coefficients are presented in the Appendix.

Analysis

The simulation model of the UFMAV was used to perform a number of analyses to assess the stability and control properties of the vehicle. These analyses do not, however, constitute a validation or verification of the simulation model since there are no static or dynamic data available for the actual aircraft in flight.

First a trim comparison is made for the vehicle in straight level flight at several dynamic pressures. The dynamic pressures (1.0, 1.6, and 2.0 psf) correspond to conditions at which experimental data are available. These data were obtained during the wind tunnel test in BART[4] and are representative of typical flight speeds of the UFMAV.

The results of three longitudinal trim studies are shown in table 2. The experimental trim results were obtained by achieving trim in the BART tunnel. This was accomplished by first setting the tunnel speed corresponding to the desired dynamic pressure and then varying the vehicle angle of attack, symmetric elevon deflection, and motor voltage (i.e., propeller rpm) until the lift was approximately equal to the gross vehicle weight and the pitching moment and total axial force were both approximately zero.

The simplified analytical trim was determined using the method described in reference 10. Equation (4) is the matrix equation that was solved to determine trim angle of attack and symmetric elevon.

$$\begin{bmatrix} C_{L_\alpha} & C_{L_{\delta_{sym}}} \\ C_{M_\alpha} & C_{M_{\delta_{sym}}} \end{bmatrix} \begin{Bmatrix} \alpha_{trim} \\ \delta_{sym_{trim}} \end{Bmatrix} = \begin{Bmatrix} \frac{W}{\bar{q}S} - C_{L_0} \\ -C_{M_0} \end{Bmatrix} \quad (4)$$

The lift curve slope, moment curve slope, and lift and moment control sensitivities were obtained from the experimental data for the corresponding dynamic

Table 2 – Experimental, analytical, and simulation based longitudinal trim.

Dynamic Pressure (psf)	Propeller RPM	Angle of Attack (deg)	Symmetric Elevon (deg)
Experimental Trim			
1.0	18,900	10.4	-6.5
1.6	20,600	5.4	-3.5
2.0	21,900	4.0	-2.5
Analytical Trim (Simplified)			
1.0	–	11.2	-5.6
1.6	–	5.4	-2.5
2.0	–	3.5	-1.9
Computed Trim (UFMAV)			
1.0	19,600	11.1	-6.8
1.6	21,200	5.6	-4.7
2.0	22,000	3.5	-1.9

Table 3 – Computed lateral-directional trim.

Dynamic Pressure (psf)	Sideslip Angle (deg)	Bank Angle (deg)	Antisymmetric Elevon (deg)
Computed Trim (UFMAV)			
1.0	-0.051	-0.97	-0.59
1.6	0.028	-1.6	-0.54
2.0	0.070	-2.1	-0.51

pressure.[4] The data was assumed to correspond to a propeller rpm near trim.

The computed trim was obtained by using the UFMAV simulation model and a constrainted optimization routine to achieve level trim at a specified dynamic pressure. Comparison of the three trim analyses shows very good agreement for angle of attack, symmetric elevon deflection, and propeller rpm. This implies that the longitudinal aerodynamic forces and moments are well approximated in the simulation.

A straight and level trim analysis using the simulation model was also performed to determine the lateral-directional quantities: sideslip, bank, and yaw angles. Table 3 shows the results of this analysis. Note that the UFMAV achieves lateral- directional control via antisymmetric elevon and dihedral coupling. It does not have two independent lateral-directional controls (such as rudder and aileron) and cannot be trimmed at zero bank angle (or zero sideslip angle) as is typical. The results indicate that though the vehicle does have significant asymmetries, all the trim values are small and within the range of values at which the aerodynamic data was obtained and are qualitatively consistent with the vehicle in flight.

Table 4 – longitudinal modes.

Dynamic Pressure (psf)	Short Period Mode		Phugoid Mode	
	damping ratio	freq. (rad/sec)	damping ratio	freq. (rad/sec)
1.0	0.13	23.3	0.44	0.85
1.6	0.12	30.2	0.35	0.65
2.0	0.12	32.6	-0.56	0.67

Table 5 – lateral-directional modes.

Dynamic Pressure (psf)	Spiral Mode	Roll Mode	Dutch Roll Mode	
	eigenvalue	eigenvalue	damping ratio	freq. (rad/sec)
1.0	-1.04	-27.7	0.094	21.1
1.6	-1.04	-37.3	0.065	24.2
2.0	-1.02	-42.8	0.050	25.9

The simulation was also linearized about the above trim conditions to assess the dynamic stability of the vehicle. Table 4 summarizes the frequency and damping of the linearized longitudinal modes. Note that the short period mode is stable for all three dynamic pressures but lightly damped. Its frequency increases with increasing dynamic pressure but the damping is essentially constant. The damping of the phugoid mode varies significantly and is unstable at the higher dynamic pressure.

Table 5 summarizes the eigenvalues or frequency and damping of the linearized lateral-directional modes. Note that all the modes are stable and that the dutch roll mode is lightly damped. This is qualitatively consistent with behavior of the vehicle in flight. Note that the spiral mode is relatively unaffected by changes in dynamic pressure but that the magnitudes of both the roll and dutch roll modes increase with increasing dynamic pressure.

Linearized models used to perform this analysis can be found in the Appendix.

Control Design

A preliminary guidance/control system has been developed to enable investigations of autonomous and collaborative control issues. The controller is composed of two main parts: an inner-loop measurement-based nonlinear dynamic inversion controller for control of angular rates and an outer-loop navigation command follower for control of wind-axis angles.[11,12] An overview of the control system is given in figure 4. The control system inputs are commanded flight-path angle γ, wind-axis heading angle χ, and total speed V_t. These inputs were chosen to allow the vehicle to be readily integrated into an existing multiple vehicle collaborative control scheme.[5] Controller outputs are commanded symmetric

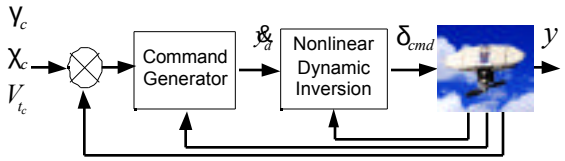

Figure 4 – structure of UFMAV control system.

and antisymmetric elevon deflection. A separate proportional-integral error loop is used to generate motor voltage commands to control total velocity. For this preliminary study, the feedback measurements are assumed to be known perfectly. The two main parts of the control system are discussed in more detail in the following.

Measurement-based Nonlinear Dynamic Inversion

Given desired values of roll acceleration $\dot{p}$, pitch acceleration $\dot{q}$, and yaw acceleration $\dot{r}$, the inner-loop controller generates symmetric and antisymmetric elevon commands to achieve the desired angular accelerations. The inner-loop controller is based on a modified nonlinear dynamic inversion approach developed in reference 11. This approach does not require a model of the baseline vehicle (i.e. no stability derivatives), but does require a model of the vehicle's control effector derivatives and feedback of body-axis angular accelerations and control effector positions. Since this approach uses acceleration measurements in lieu of a complete on-board vehicle model, this approach is less sensitive to vehicle model errors and can adapt to vehicle failures and/or damage. An overview of the approach from reference 11 is given in the following.

Given the vehicle equations of motion

$$\begin{aligned} \dot{x} &= F(x,\delta) = f(x) + g(x,\delta) \\ y &= \begin{bmatrix} p & q & r \end{bmatrix}^T = h(x) \end{aligned} \tag{5}$$

where x is the vehicle state vector, δ is the vehicle control vector, and y is the vector of control variables: roll rate p, pitch rate q, and yaw rate r. A Taylor series expansion of (5) yields the following first-order approximation to $F(x,\delta)$ in the neighborhood of $\begin{bmatrix} x_0, \delta_0 \end{bmatrix}$

$$\begin{aligned} F(x,\delta) = {} & f(x_0) + g(x_0,\delta_0) + \\ & \frac{\partial}{\partial x}\Big(f(x) + g(x,\delta)\Big)\Big|_{x=x_0,\delta=\delta_0} (x - x_0) \\ & \frac{\partial}{\partial \delta}\Big(g(x,\delta)\Big)\Big|_{x=x_0,\delta=\delta_0} (\delta - \delta_0) \end{aligned} \tag{6}$$

Letting x_0 and δ_0 denote a previous state and control from the recent past and defining

$$\begin{aligned} A_0 &= \frac{\partial}{\partial x}\Big(f(x) + g(x,\delta)\Big)\Big|_{x=x_0,\delta=\delta_0} \\ B_0 &= \frac{\partial}{\partial \delta}\Big(g(x,\delta)\Big)\Big|_{x=x_0,\delta=\delta_0} \end{aligned} \tag{7}$$

$F(x,\delta)$ can be written as

$$F(x,\delta) = \dot{x} \quad \dot{x}_0 + A_0(x - x_0) + B_0\Delta\delta \tag{8}$$

in the neighborhood of $x = x_0$, $\delta = \delta_0$ where $\delta = \delta_0 + \Delta\delta$.

At this point, this development differs from reference 11 in that the number of controls is less than the number of controlled variables and so the desired responses cannot be completely achieved. A control law is obtained by minimizing

$$J = (\dot{y}_d - \dot{y})^T Q(\dot{y}_d - \dot{y}) \tag{9}$$

where

$$\dot{y} = \frac{\partial h(x)}{\partial x}\dot{x} = h_x\left(\dot{x}_0 + A_0(x - x_0) + B_0\Delta\delta\right) \tag{10}$$

and Q is a positive-definite diagonal weighting matrix used to emphasize desired system responses. This yields

$$\begin{aligned} \Delta\delta = {} & \left[(h_x B_0)^T Q h_x B_0\right]^{-1} (h_x B_0)^T Q \\ & \left(\dot{y}_d - h_x \dot{x}_0\right) \end{aligned} \tag{11}$$

With a sufficiently fast update rate x tends to x_0 and equation (11) becomes

$$\Delta\delta = \left[(h_x B_0)^T Q h_x B_0\right]^{-1} (h_x B_0)^T Q\left(\dot{y}_d - h_x \dot{x}_0\right) \tag{12}$$

where $\delta = \delta_0 + \Delta\delta$. The vehicle's control derivatives B_0 are generated from the nonlinear aerodynamic control coefficients using a central difference approximation.

Navigation Command Follower

Given desired values of flight path angle γ, wind-axis heading χ, and total velocity V_t the navigation command follower generates required roll rate, pitch rate, and yaw rate acceleration commands for the inner-loop controller.

The desired dynamics for the outer-loop were chosen to be

$$\dot{\gamma}_d = \omega_\gamma(\gamma_c - \gamma)$$
$$\dot{\chi}_d = \omega_\chi(\chi_c - \chi) \tag{13}$$

where the subscript d denotes the desired value and the subscript c denotes commanded input values. The bandwidths ω_χ and ω_γ were chosen to be approximately a decade below the bandwidths of the desired inner-loop dynamics and therefore were chosen to be 2 rad/sec.

Using the wind-axis point mass equations of motion and assuming sideslip angle and sideforce are small and that V_t and $cos(\gamma)$ are non-zero, commanded wind-axis bank angle μ_c can be determined as a function of V_t, $\dot{\gamma}_d$ and $\dot{\chi}_d$ [13]

$$\tan\mu_c = \frac{V_t\dot{\chi}_d\cos\gamma}{V_t\dot{\gamma}_d + g\cos\gamma} \tag{14}$$

The desired dynamics for wind-axis bank angle was chosen to be

$$\dot{\mu}_d = \omega_\mu(\mu_c - \mu) \tag{15}$$

where ω_μ were chosen to be 4 rad/sec.

The wind-axis angular rates $\dot{\mu}$, $\dot{\gamma}$, and $\dot{\chi}$ are transformed to commanded body-axis rates (assuming sideslip angle is zero) using

$$\begin{Bmatrix} p_c \\ q_c \\ r_c \end{Bmatrix} = \begin{bmatrix} \cos\alpha & 0 & -\sin\alpha \\ 0 & 1 & 0 \\ \sin\alpha & 0 & \cos\alpha \end{bmatrix} \begin{bmatrix} 1 & 0 & -\sin\gamma \\ 0 & \cos\mu & \sin\mu\cos\gamma \\ 0 & -\sin\mu & \cos\mu\cos\gamma \end{bmatrix} \begin{Bmatrix} \dot{\mu} \\ \dot{\gamma} \\ \dot{\chi} \end{Bmatrix} \tag{16}$$

where α is angle of attack. The desired closed-loop dynamics $\dot{y}_d$ for the inner-loop were chosen to be

$$\dot{p}_d = \omega_p(p_c - p)$$
$$\dot{q}_d = \omega_q(q_c - q) \tag{17}$$
$$\dot{r}_d = \omega_r(r_c - r)$$

where the subscript d denotes the desired value and the subscript c denotes commanded values determined by the outer-loop control law. The inner-loop bandwidths ω_p, ω_q, ω_r were chosen to be 20, 15 and 20 rad/sec, respectively, consistent with the open-loop bandwidth.

Figure 6 shows time responses for inner-loop p_c, q_c, and r_c angular rate commands (i.e. no outer-loop controller). The initial condition for these time responses is straight and level flight at V_t = 37 feet/sec. Reference signals were generated for comparison with the achieved responses from equations (13), (15), and (17) using the specified bandwidths. The commands and reference signals are shown respectively as dashed and dotted lines in the upper two plots of figures 6a and 6b. A stability-axis roll rate doublet was commanded (50 deg/sec from 1 to 2 seconds and –50 deg/sec from 2 to 3 seconds) with pitch rate and stability-axis yaw rate commanded to zero. The effect of choice of control variable weighting is demonstrated in these figures. Figure 6a shows responses for a control variable weighting of Q = diag([roll acceleration error weighting, pitch acceleration error weighting, yaw acceleration error weighting]) = diag([1,5,2]). As can be seen, the stability-axis roll rate

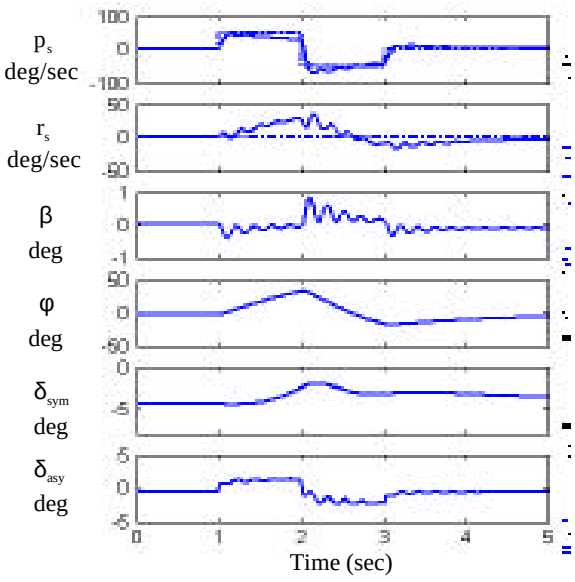

Figure 6a – inner-loop p_c, q_c, and r_c angular rate commands, Q = diag([1,5,2]).

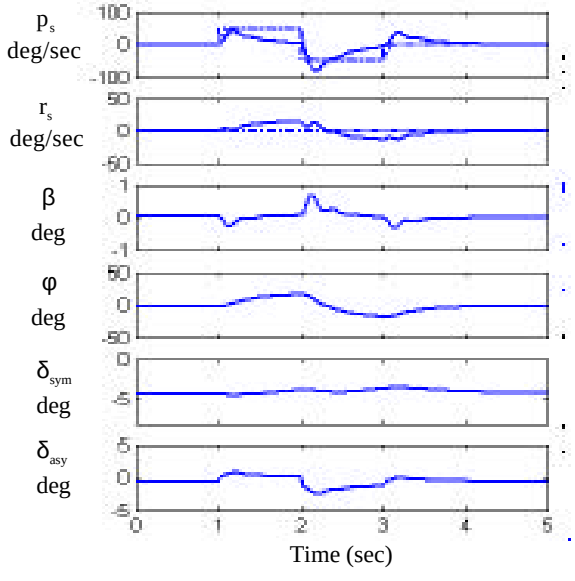

Figure 6b – inner-loop p_c, q_c, and r_c angular rate commands, Q = diag([1,5,10]).

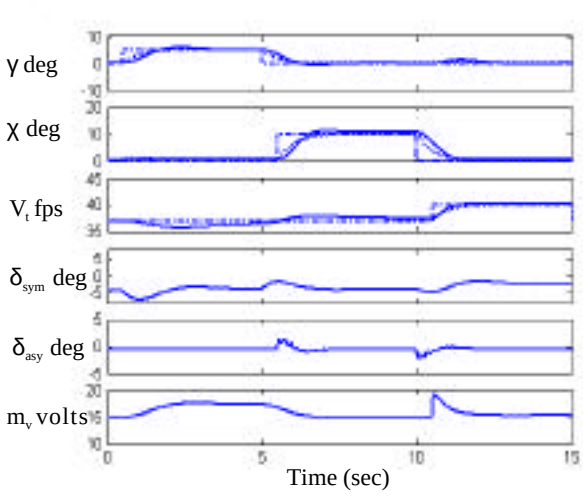

Figure 7 - Figure 3 – outer-loop γ_c, χ_c, and V_{t_c} commands, Q = diag([1,5,2]).

reference signal is more closely followed than the stability-axis yaw rate reference signal with low dutch roll damping as illustrated by the oscillatory sideslip response. Figure 6b shows responses for Q = diag([1,5,10]). This results in the stability-axis yaw rate reference signal being more closely followed than in figure 6a and a better damped sideslip response.

Figure 7 shows time responses for outer-loop γ_c, χ_c, and V_{t_c} commands. The control variable weighting was Q = diag([1,5,2]). The commanded and reference signal values are shown respectively as dashed and dotted lines in the top three plots. As can be seen, the vehicle closely follows the reference signal with reasonable control activity.

These preliminary results demonstrate that this is a viable approach for control of systems where the number of controls is less than the number of control variables, such as, MAV's. Future efforts will focus on improvements to this approach, robustness analysis, and use of this method as part of a multiple vehicle collaborative control scheme.

Concluding Remarks

A dynamic simulation model of an aeroelastic fixed wing micro aerial vehicle has been developed that is suitable for a wide variety of uses including control system design, navigation and guidance algorithm development, and their assessment. The simulation is based on a vehicle concept developed at the University of Florida and wind-tunnel data collected in the NASA Langley Basic Aerodynamics Research Tunnel. Regression analysis was used to obtain a generalized Taylor series aerodynamic model.

The simulation was used to assess vehicle trim and basic stability and control properties. The analysis indicates that the vehicle has acceptable stability properties and good controllability.

A control system was designed using a measurement-based nonlinear dynamic inversion approach. The method was extended to accommodate application to systems with fewer controls than controlled variables as is the case for the subject vehicle. A guidance loop was also designed to allow the simulation model to be integrated into an existing multiple vehicle collaborative framework.

Assessment of the control and guidance systems using the simulation demonstrated satisfactory performance. Additional research is underway to improve the dynamic response, investigate performance robustness, and explore implementation issues.

Acknowledgements

The authors wish to acknowledge Matt Pfenninger, Blain Levedahl, Matthew Lackner, and Jonathan Cook for their assistance in developing and documenting the simulation.

References

[1] Mueller, T. J. editor, "Proceedings of the Conference on Fixed, Flapping and Rotary Wing Vehicles at Very Low Reynolds Numbers," Notre Dame University, Indiana, June 5-7, 2000.

[2] Ifju, P.G., Jenkins, D.A., et.al., "Flexible–Wing–Based Micro Air Vehicles," AIAA Paper No. 2002-0705. AIAA Aerospace Sciences Meeting, Reno, NV, January 2002.

[3] Ifju, P.G., Ettinger, S., Jenkins, D.A., and Martinez, L.," Society for the Advancement of Materials and Process Engineering Annual Conference, Long Beach, CA, May 6-10, 2001.

[4] Waszak, M.R., Jenkins, L.N., and Ifju, P.J., "Stability and Control Properties of an Aeroelastic Fixed Wing Micro Aerial Vehicle." AIAA Paper 2001-4005. Presented at the 2001 AIAA Atmospheric Flight Mechanics Conference. Montreal, Canada. August 2001.

[5] Anderson, M.R. and Robbins, A.C., "Formation Flight as a Cooperative Game," AIAA Paper Number AIAA-98-4124. Presented at the 1998 AIAA Guidance, Navigation, and Control Conference. Boston, MA. August 1998.

[6] Stevens, B.L. and Lewis, F.L., *Aircraft Control and Simulation*. John Wiley and Sons, Inc., 1992.

[7] Anon., *Using Simulink: Version 2*. The Math Works, Inc. Natick, Mass., January 1997.

[8] Ashby, D.L., "Potential Flow Theory and Operation Guide for the Panel Code PMARC_14," NASA TM-1999-209582, December 1999.

[9] Blakelock, J.H., *Automatic Control of Aircraft and Missiles*. John Wiley & Sons, Inc., 1965.

[10] Etkin, B., *Dynamics of Atmospheric Flight*. John Wiley and Sons, Inc., 1972.

[11] Bacon, B.J. and Ostroff, A.J., "Reconfigurable Flight Control using Nonlinear Dynamic Inversion with a Special Accelerometer Implementation," AIAA Paper 2000-4565, AIAA Guidance, Navigation and Control Conference, Denver, CO, August 2000.

[12] Snell, S.A., Enns, D.F., and Garrard, W.L., "Nonlinear Inversion Flight Control for a Supermaneuverable Aircraft," AIAA Paper 90-3406-CP, AIAA Guidance, Navigation and Control Conference, Portland, OR, August 1990.

[13] Snell, S.A., Enns, D.F., and Garrard, W.L., "Nonlinear Control of a Supermaneuverable Aircraft," AIAA Paper 89-3486-CP, AIAA Guidance, Navigation and Control Conference, Boston, MA, August 1989.

Appendix

The appendix contains a block diagram of the basic structure of the simulation model, tables of the aerodynamic force and moment coefficients and linearized models of the UFMAV.

Simulation Block Diagram

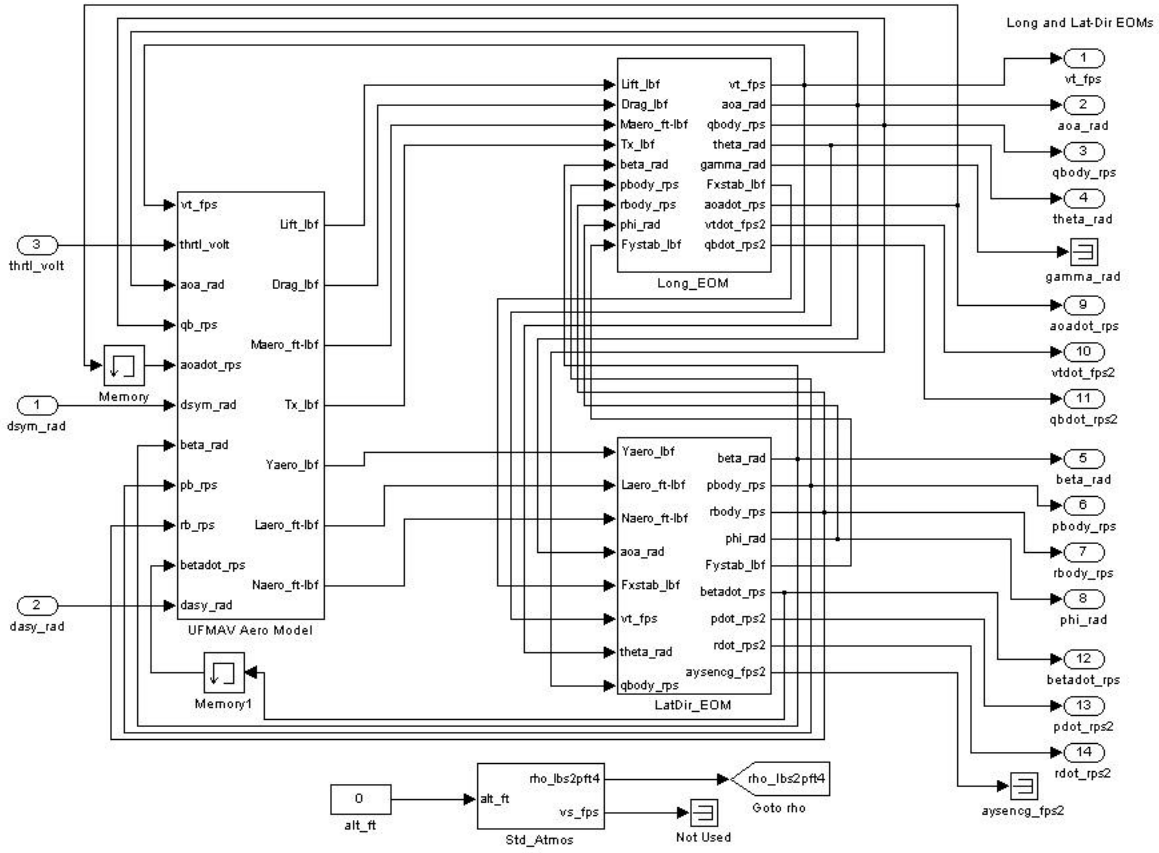

Aerodynamic Force/Moment Coefficients

Longitudinal Axes

Lift Coefficient	q = 1.0 (psf)	q = 1.6 (psf)	q = 2.0 (psf)
C_{L_0}	0.36094	0.341	0.344
C_{L_α}	3.1365	2.95	2.94
$C_{L_{\delta_{sym}}}$	0.65369	0.590	0.590
C_{L_T}	0.0043367	0.00306	0.00169
$C_{L_{\alpha T}}$	0.035346	0.0331	0.0228
$C_{L_{\delta_{sym}T}}$	0.012241	0.00721	0.00394
C_{L_q}	4.0	4.0	4.0
$C_{L_{\dot{\alpha}}}$	1.0	1.0	1.0

Drag Coefficient	q = 1.0 (psf)	q = 1.6 (psf)	q = 2.0 (psf)
C_{D_0}	0.150	0.162	0.157
C_{D_α}	0.304	0.257	0.166
$C_{D_{\delta_{sym}}}$	0.0335	0.0462	0.0281
C_{D_T}	-4.13e-3	-6.46e-4	0.0843
$C_{D_{\alpha^2}}$	2.99	3.14	3.43
$C_{D_{\delta_{sym}^2}}$	0.224	0.202	0.182
$C_{D_{T^2}}$	2.99e-4	8.24e-5	-3.83e-3
$C_{D_{\alpha\delta_{sym}}}$	0.648	0.731	0.659

Pitch Moment Coefficient	q = 1.0 (psf)	q = 1.6 (psf)	q = 2.0 (psf)
C_{m_0}	0.0797	0.0321	0.0304
C_{m_α}	-0.470	-0.702	-0.741
$C_{m_{\delta_{sym}}}$	-0.350	-0.384	-0.355
C_{m_T}	2.61e-4	1.26e-4	-4.86e-5
$C_{m_{\alpha\delta_{sym}}}$	0.14493	0.0884	0.136
$C_{m_{\alpha T}}$	-0.0118	-2.01e-3	0.00206
$C_{m_{\delta_{sym}T}}$	-5.51e-3	-4.52e-3	-2.52e-3
C_{m_q}	-0.5	-0.5	-0.5
$C_{m_{\dot{\alpha}}}$	-3.0	-3.0	-3.0

Lateral-Directional Axes

Coefficient	Sideforce (Y)	Rolling Moment (l)	Yawing Moment (n)
$C_{(\cdot)_0}$	-1.91e-2	-4.72e-3	5.73e-3
$C_{(\cdot)_\beta}$	-8.55e-1	-2.74e-1	-3.25e-1
$C_{(\cdot)_{\delta_{asy}}}$	-5.72e-2	6.00e-2	3.00e-2
$C_{(\cdot)_T}$	1.83e-3	2.70e-4	-2.46e-4
$C_{(\cdot)_{\delta_{asy}T}}$	-3.57e-3	1.25e-3	1.82e-3
$C_{(\cdot)_{\beta T}}$	-2.15e-2	-4.09e-3	-3.33e-3
$C_{(\cdot)_{pbody}}$	-0.35	-0.65	-0.015
$C_{(\cdot)_{rbody}}$	1.3	-0.32	-0.5

Motor and Thrust Models

Motor Coefficient	Value
C_{M_0}	2.17
$C_{M_{\bar{q}}}$	0.0793
$C_{M_{v_{motor}}}$	-0.0620
$C_{M_{v^2_{motor}}}$	0.000293
C_{M_α}	-0.0264
$C_{M_{\alpha^2}}$	-0.179

Thrust Coefficient	Value
C_{T_1}	-0.00140
C_{T_2}	0.000129

Linear Models

Longitudinal Axis

input vector: $u^T = [\delta_{sym}\ v_{motor}]$

state vector: $x^T = [V_t\ \alpha\ q\ \theta]$

q = 1.0 psf

$$A = \begin{bmatrix} -1.17 & -11.3 & 0 & -32.2 \\ -0.0602 & -4.02 & 0.982 & 2.99e-5 \\ -5.14 & -545. & -1.80 & 0 \\ 0 & 0 & 1.0 & 0 \end{bmatrix}$$

$$B = \begin{bmatrix} -2.92 & 1.61 \\ -0.852 & -0.0193 \\ -327. & -0.764 \\ 0 & 0 \end{bmatrix}$$

$$B = \begin{bmatrix} -0.121 & 0.00136 \\ 385 & 0.624 \\ 167 & -0.179 \\ 0 & 0 \end{bmatrix}$$

q = 1.6 psf

q = 1.6 psf

$$A = \begin{bmatrix} -0.648 & -6.55 & 0 & -32.2 \\ -0.0355 & -4.67 & 0.982 & 3.40e-5 \\ -4.43 & -915. & -2.28 & 0 \\ 0 & 0 & 1.0 & 0 \end{bmatrix}$$

$$A = \begin{bmatrix} -1.58 & 0.0954 & -0.985 & 0.873 \\ -2020 & -28.5 & -17.8 & 0 \\ 261 & -5.27 & -11.4 & 0 \\ 0 & 1.0 & 0.0987 & 0 \end{bmatrix}$$

$$B = \begin{bmatrix} -3.76 & 1.23 \\ -0.896 & -0.00814 \\ -573. & 0.238 \\ 0 & 0 \end{bmatrix}$$

$$B = \begin{bmatrix} -0.160 & 0.00148 \\ 632 & 0.893 \\ 277 & -0.270 \\ 0 & 0 \end{bmatrix}$$

q = 2.0 psf

q = 2.0 psf

$$A = \begin{bmatrix} -0.670 & -4.5 & 0 & -32.2 \\ -0.0247 & -4.87 & 0.982 & 3.14e-5 \\ -2.38 & -1067. & -2.55 & 0 \\ 0 & 0 & 1.0 & 0 \end{bmatrix}$$

$$A = \begin{bmatrix} -1.79 & 0.0587 & -0.987 & 0.782 \\ -2562 & -31.2 & -19.9 & 0 \\ 313 & -5.89 & -12.8 & 0 \\ 0 & 1.0 & 0.0617 & 0 \end{bmatrix}$$

$$B = \begin{bmatrix} -3.12 & 4.16 \\ -0.912 & -0.00428 \\ -612. & 0.161 \\ 0 & 0 \end{bmatrix}$$

$$B = \begin{bmatrix} -0.183 & 0.00148 \\ 802 & 1.07 \\ 354 & -0.334 \\ 0 & 0 \end{bmatrix}$$

Lateral-Directional Axis

input vector: $u^T = [\delta_{asy} \; v_{motor}]$

state vector: $x^T = [\beta \quad p \quad r \quad \varphi]$

q = 1.0 psf

$$A = \begin{bmatrix} -1.22 & 0.189 & -0.971 & 1.09 \\ -1230 & -22.5 & -14.1 & 0 \\ 177 & -4.17 & -9.01 & 0 \\ 0 & 1.0 & 0.196 & 0 \end{bmatrix}$$